Power Flow Control Based Solely on Slow Feedback Loop for Heart Pump Applications

Bob Wang, *Graduate Student Member, IEEE*, Aiguo Patrick Hu, *Senior Member, IEEE*, and David Budgett

***Abstract*—This paper proposes a new control method for regulating power flow via transcutaneous energy transfer (TET) for implantable heart pumps. Previous work on power flow controller requires a fast feedback loop that needs additional switching devices and resonant capacitors to be added to the primary converter. The proposed power flow controller eliminates these additional components, and it relies solely on a slow feedback loop to directly drive the primary converter to meet the heart pump power demand and ensure zero voltage switching. A controlled change in switching frequency varies the resonant tank shorting period of a current-fed push-pull resonant converter, thus changing the magnitude of the primary resonant voltage, as well as the tuning between primary and secondary resonant tanks. The proposed controller has been implemented successfully using an analogue circuit and has reached an end-to-end power efficiency of 79.6% at 10 W with a switching frequency regulation range of 149.3 kHz to 182.2 kHz.**

***Index Terms*—Analogue circuits, biomedical electronics, implantable devices, power flow control, resonant inverters, transcutaneous energy transfer (TET).**

I. Introduction

EXISTING implanted heart pumps are powered by a percutaneous cable, which is a major source of infection [1]. Wireless power transfer [2]–[4] is capable of power delivery between two physically isolated coils, when one coil is inside the body, and the second outside the body, the technique is termed transcutaneous energy transfer (TET). For heart pumps, TET is capable of transferring power across the intact skin and eliminating the percutaneous power cable and its associated risks. The major issues facing TET is dealing with variations in coil coupling and heating. Dissanayake *et al.* [5], [6] have shown that 15 W, suitable for powering a heart pump, can be transferred into the body of sheep with maximum temperature rise of approximately 4°C. A power flow controller needs to be in place to compensate for coupling variations and ensure the heart pump is always receiving the required power level. Si *et al.* have proposed a variable resonant frequency method [7] to regulate the power flow by changing the effective capacitance of the primary through switching in and out parallel capacitors to the primary MOSFETs. Dissanayake *et al.* [6] successfully implemented this frequency control in a TET system for powering heart pumps. This requires the system to have more switching devices and resonant capacitors.

Thrimawithana *et al.* [8]–[12] have proposed and analysed a split capacitor push-pull parallel resonant converter (SC-PPRC) in three different operational modes, namely buck, normal and boost modes. The SC-PPRC changes its frequency and duty cycle simultaneously to achieve zero voltage switching (ZVS) condition at a range of operational frequencies, the SC-PPRC can regulate power flow by varying the primary switching frequency directly. The boost version of SC-PPRC attains its name because as frequency reduces the peak resonant voltage would increase.

Here we extend the boost version of SC-PPRC and propose a new frequency controller operating solely via a slow feedback loop for TET systems to deliver rated power for implanted heart pumps. The switching frequency regulation range is chosen to ensure a monotonic relationship between frequency and power flow, this allows the use of simple proportional and integral control to set the system switching frequency. The switching frequency is always below the system's lowest resonant tank zero voltage switching frequency, leading to resonant tank shorting and ZVS during MOSFET commutation without the need of fast detection circuitry. This controller also offers the advantage of reduced switching components and capacitors compared to the variable frequency circuit of Dissanayake *et al.* [6].

II. System Overview

Fig. 1 shows the proposed TET system with a proportional and integral (PI) controller. The system includes a push-pull parallel tuned resonant converter to invert a dc input voltage into a high frequency current flowing through a primary coil. A secondary pickup coil (with a quality factor Q of about 165) is coupled to the primary coil (with a quality factor Q of about 205) by magnetic induction. Then the pickup coil is parallel tuned and the induced voltage rectified to output a dc voltage to drive the load.

The load voltage is detected and sent back to the controller via a RF channel, this makes use of the already available RF channel used for physiological sensors in an implantable heart pump application. The proposed controller compares the received feedback information with a pre-set reference V_{ref}, and the difference is regulated by the PI controller to generate a dc signal,

Manuscript received March 31, 2011; revised July 23, 2011; accepted September 18, 2011. Date of publication November 23, 2011; date of current version May 22, 2012. This paper was recommended by Associate Editor T. Denison.

B. Wang and A. P. Hu are with the Department of Electrical and Computer Engineering, The University of Auckland, Auckland 1142, New Zealand (e-mail: bwan033@aucklanduni.ac.nz; a.hu@auckland.ac.nz).

D. Budgett is with the Bioengineering Institute, The University of Auckland, Auckland 1010, New Zealand and also with Telemetry Research Limited, Auckland 1141, New Zealand (e-mail: d.budgett@auckland.ac.nz).

Color versions of one or more of the figures in this paper are available online at http://ieeexplore.ieee.org.

Digital Object Identifier 10.1109/TBCAS.2011.2171689

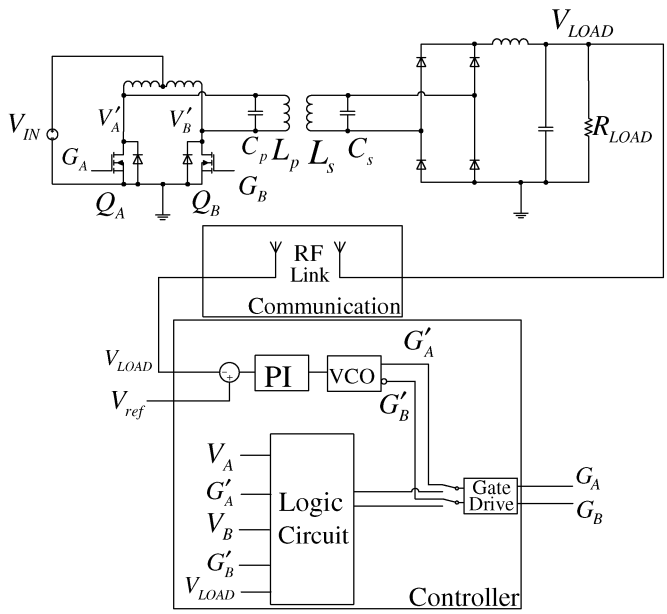

Fig. 1. System overview.

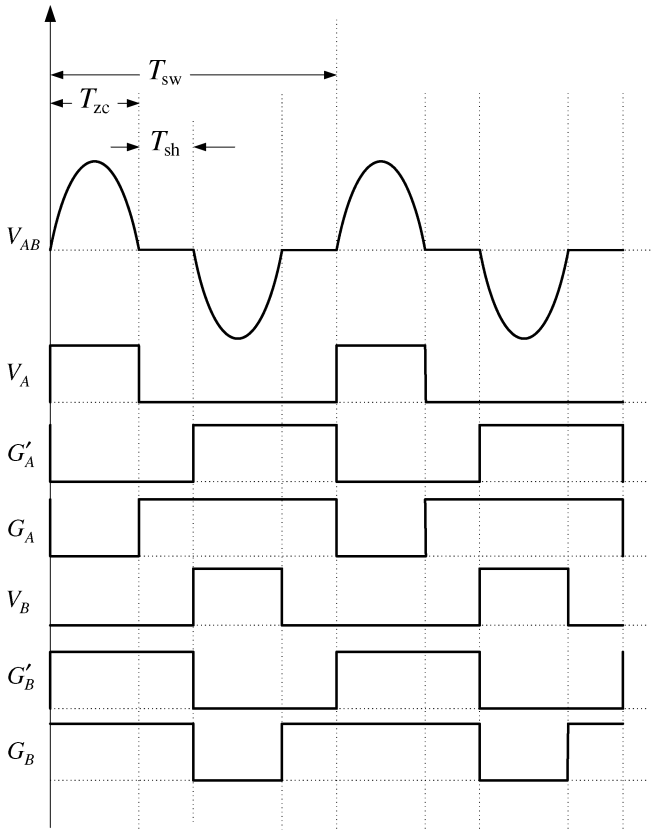

Fig. 2. Circuit ideal waveforms.

which is fed into a voltage controlled oscillator (VCO) to generate gate drive signals G'_A and G'_B (inversion of G'_A) at a certain frequency.

The controller can operate in two separate gate drive modes by a manual selection switch: the basic mode and enhanced mode. In the basic mode, G'_A and G'_B are used to drive the two MOSFETs directly at 50% duty cycle after a gate drive circuit. One of the body diodes of the two MOSFETs would be conducting if the resonant tank needs to be shorted as will be discussed later. The basic mode is the mode that this paper claims to be based solely on slow feedback PI loop, as it does not require any fast detection, this can be beneficial and simplifies the speed and timing requirement of the feedback channel and its components. Alternatively, in the enhanced mode, both MOSFETs would be ON during resonant tank shorting period to reduce the voltage drop of the body diodes and improve the power efficiency slightly. However the enhanced mode requires an additional logic circuit that would require fast detection for resonant tank voltage as shown in Fig. 1.

Fig. 2 illustrates the ideal circuit waveforms of the proposed system. V_{AB} is the differential resonant tank waveform measured from across the resonant capacitor, V_A and V_B are comparator results of MOSFET drain to source voltages (V'_A and V'_B) with respect to ground. The primary MOSFETs Q_A and Q_B can either be driven by the basic mode, G'_A and G'_B, which are simply the VCO outputs or by the enhanced mode, G_A and G_B.

In the basic gate driving mode, the MOSFET body diodes will take turns to conduct during consecutive resonant tank shorting periods (T_{sh}), note that T_{sh} occurs twice every switching period (T_{sw}), T_{zc} is the zero crossing period, which is the duration in between two T_{sh}. In enhanced gate drive mode, MOSFETs' body diodes will cease to conduct as both MOSFETs are ON simultaneously during all T_{sh}.

Instant capacitor shorting must be avoided to prevent damage to switching components. It will occur whenever MOSFETs are switched ON where there is a voltage present across resonant capacitor leading to an unwanted high shorting current.

Instant capacitor shorting must not be confused with resonant tank shorting in the proposed controller. Resonant tank shorting occurs when MOSFETs are driven with a system switching frequency (f_{sw}) that is below the lowest system zero voltage switching frequency (f_{zvs}), which means the resonant tank will resonate and then be shorted for a short period by a current loop formed by the two MOSFETs including their body diodes if basic mode control is employed.

III. Determination of Switching Frequency Regulation Range

A. Finding System ZVS Frequency

It is necessary to find the f_{zvs} points of the system in order to determine an operating frequency range that avoids instant capacitor shorting. If the harmonics generated by the inverter is ignored, the system f_{zvs} points are found at zero phase angles of the resonant tank impedance. This is when the complex part of the impedance equals zero, and it means the inductive and capacitive elements cancel each other making the impedance purely resistive. Changes in system parameters can impact on the number of f_{zvs} points as well as their actual values. The most influential system parameters on the power flow of the proposed TET system are the load and coupling level. Under cer-

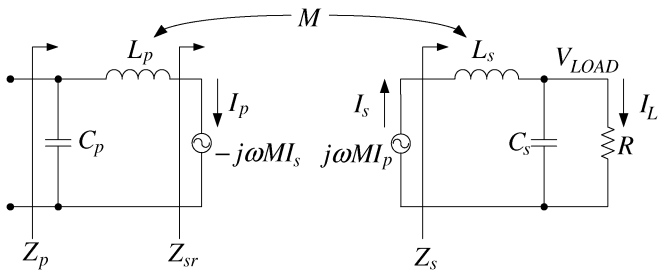

Fig. 3. Circuit used to find the impedance phase angle.

tain conditions, the system will have more than one zero voltage switching frequency, causing system to bifurcate. Similar bifurcation phenomena have also been found and studied in resonant converters in other wireless power transfer systems [13]–[17].

The circuit f_{zvs} can be found by applying impedance analysis on the primary and secondary resonant tanks including load as shown in Fig. 3, the secondary impedance (Z_s) is reflected to primary in series with the primary TET coil inductance shown as Z_{sr}. First we find the resonant tank input impedance (Z_p), then by equating the complex components of Z_p to zero, the phase plot zero crossing points can be calculated through MATLAB using (1) giving the approximate system f_{zvs} points.

$$\begin{aligned}&\omega^6 C_p C_s^2 R^2 (L_p L_s - M^2)^2 - \omega^4 (L_p L_s - M^2)\\ &\times \left[L_p C_p C_s R^2 + C_s R^2 (L_p C_p + L_s C_s) - C_p (L_p L_s - M^2)\right]\\ &-\omega^2 \left[L_s (L_p L_s - M^2) - L_p R^2 (L_p C_p + L_s C_s)\right.\\ &\qquad \left. - C_s R^2 (L_p L_s - M^2)\right] - L_p R^2 = 0 \end{aligned} \tag{1}$$

There are two graphical approaches to find f_{zvs}, firstly and more conveniently LTspice can frequency sweep the circuit in Fig. 3 to give phase plots of Z_p, the induced voltages from primary to secondary and vice versa need not be included during LTspice simulations as they are integral part of L_p and L_s. To represent the system more accurately, primary and secondary equivalent series resistances of capacitances and inductances are included. Secondly, MATLAB can plot f_{zvs} bifurcation trends while stepping load or coupling coefficient.

To differentiate between non-bifurcated and bifurcated system operating conditions, Fig. 4 shows a single phase plot zero crossing meaning one f_{zvs} point, while Fig. 5 shows three phase plot zero crossings indicating f_{zvs} bifurcation with three f_{zvs} points.

B. Switching Frequency Regulation Range

Instant capacitor shorting is to be avoided, it occurs at negative resonant tank impedance phase angles, and thus we must constrain the system to operate in a f_{sw} regulation range with positive phase angles. The system can either operate in non-bifurcated or bifurcated conditions. Fig. 4 shows the phase angle and magnitude plot for a non-bifurcated condition, phase angle is positive when f_{sw} is below f_{zvs} and is negative when f_{sw} is above f_{zvs}. During a bifurcated condition as shown by Fig. 5, there are three f_{zvs} points, with positive phase angles when

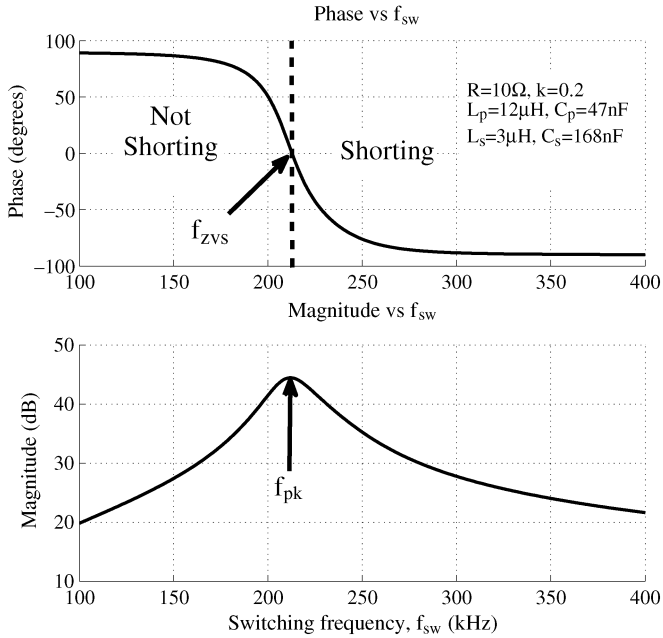

Fig. 4. Phase and magnitude sweep of a non-bifurcated system.

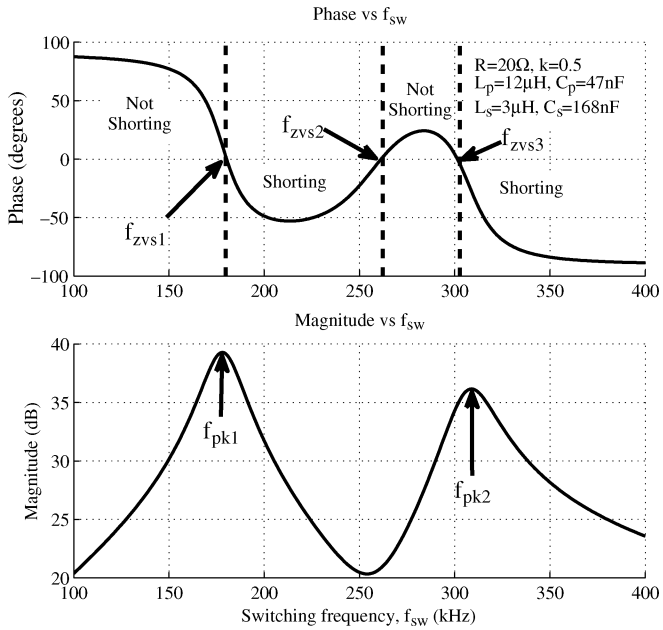

Fig. 5. Phase and magnitude sweep of a bifurcated system.

f_{sw} falls below f_{zvs1} or in between f_{zvs2} and f_{zvs3}. The frequency range between f_{zvs2} and f_{zvs3} may be utilised in theory since it has positive phase angles and will avoid instant capacitor shorting, but this frequency range is variable under different loading and coupling conditions, it is difficult to track its bounds, so we will avoid operating inside that range. Therefore, in both non-bifurcated and bifurcated conditions, the f_{sw} regulation range must be less than or equal to the lowest f_{zvs}.

In addition, the upper boundary of f_{sw} regulation range is affected by the magnitude frequency response of the system. A magnitude frequency sweep of either secondary output load voltage (V_{LOAD}) or Z_p in Fig. 3 will give the first system peak power flow frequency (f_{pk}), which is always less than or equal

to the lowest f_{zvs}. When the system approaches bifurcation or is in a bifurcated condition, there will be two f_{pk} rather than the single f_{pk} in a non-bifurcated condition. The first f_{pk} tend to decrease as system becomes more bifurcated. This creates a power flow trough in between the f_{pk} points as shown in Fig. 5. In order to maintain monotonicity in negative feedback, the system must maintain operation with a positive magnitude over frequency slope, and operate below the first f_{pk} where the slope is always positive. Therefore, the upper boundary of f_{sw} regulation range should be set to the first f_{pk} to prevent PI tracking in the wrong direction.

The lower boundary of f_{sw} regulation range will be affected by a resonant tank voltage boosting effect in the converter as f_{sw} range decreases. Despite the differences between the proposed controller and SC-PPRC, the analysis done by Thrimawithana *et al.* [8], [9] for boost mode SC-PPRC can be used to explain the boosting effect. Varying f_{sw} has two effects on power flow, the dominating effect in the proposed controller is frequency tuning and detuning as f_{sw} moves toward and away from f_{pk}, the lesser effect is change in resonant tank peak voltage (V_{pk}) and resonant tank RMS voltage (V_{rms}) with f_{sw}, an increase in switching period (T_{sw}) will lead to an increase in V_{rms} as shown in (2) leading to increased power transfer

$$V_{\rm rms} = \frac{1}{2}\pi V_{DC}\sqrt{\frac{T_{sw}}{T_{zc}}}. \tag{2}$$

In addition, because f_{sw} reduces with increase in T_{sw}, the system will become increasingly detuned with a dropping power flow. However V_{rms} will be increasing to rise the power flow, these two power flow effects will superpose and there will be a cross over point when the magnitude boosting effect overrides frequency tuning effect, this point shall be set as the lower f_{sw} boundary to maintain the monotonic relationship between power flow and f_{sw}.

The Q of the system will affect the frequency regulation range. If Q is increased, it means the magnitude is more sensitive to changes in frequency, and then to maintain the same variation in magnitude, the frequency range would be narrower. On the contrary, if Q is decreased, the frequency range would need to be wider.

C. Phase Plot Trends and Bifurcation Plots

At increased loading or coupling level, bifurcation results when number of phase zero crossing points increase from one to three. The magnitude frequency response begins to show a trough with two f_{pk} emerging on bifurcation rather than the single f_{pk} when there is no bifurcation. A series of phase plots can be portrayed through a bifurcation trend plot, which shows f_{zvs} points while a system parameter is being stepped. When the primary and secondary resonant tanks are tuned to nominal frequency (f_N), with increased loading or coupling level leading to f_{zvs} bifurcation, two additional f_{zvs} emerge on either side of original f_{zvs}, these two points will depart from the original f_{zvs}, with one rising and the other falling in frequency.

Understanding the phase plot trends during system transits from a non-bifurcated condition to a bifurcated condition can help increase f_{sw} regulation range and avoid instant capacitor shorting. As shown in Fig. 6, if secondary resonant capacitance (C_s) was chosen to be below C_{sN}, which is the capacitance that tunes the secondary resonant tank to f_N, at increased load or coupling level leading to f_{zvs} bifurcation, the two additional f_{zvs} points will emerge above the original f_{zvs} and will not interfere with controller operations since the f_{sw} is designed to be always below the original f_{zvs}. In the other two bifurcation cases, one being C_s close to C_{sN} or C_s greater than C_{sN}, at least one f_{zvs} point emerges below original f_{zvs}, this means in order to avoid instant capacitor shorting, we need to lower upper frequency boundary resulting in a smaller f_{sw} regulation range.

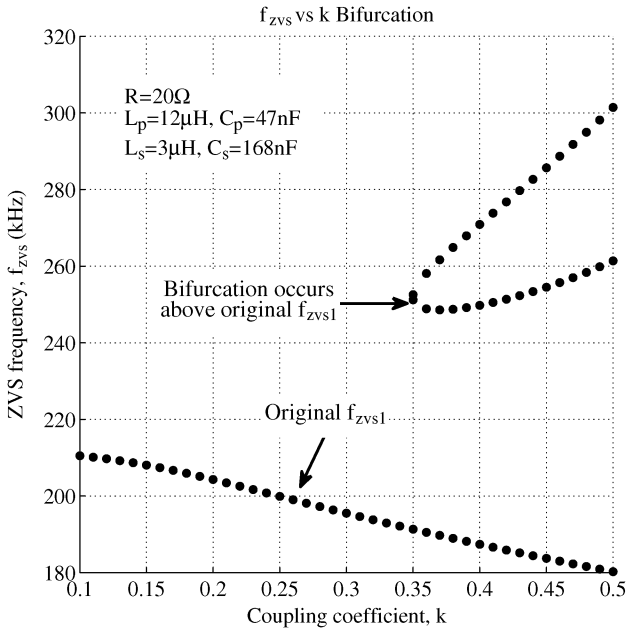

Fig. 6. Bifurcation plot for reduced C_s.

Coupling level increase spreads bifurcated f_{zvs} points further apart leading to a lower first system f_{pk}. Decreasing C_s will counter this by shifting the entire phase plot to a higher frequency leading to higher first f_{pk} and a larger f_{sw} regulation range. The trade-off is detuning the primary and secondary tanks slightly and thus requiring a higher dc source voltage at the inverter input.

IV. Controller Design

A. Finding Switching Frequency Regulation Range

Highest coupling level and heaviest load need to be considered in finding the f_{sw} regulation range, as this will give the worst case scenario giving the lowest expectable first f_{pk} on bifurcation. We shall constrain the system to work below this worst case first f_{pk} and above the f_{sw} when magnitude boosting effect overrides frequency tuning effect. The practical TET coils used for the primary and secondary are encased in silicone with the same diameter of 50 mm, but the primary is double layered and secondary is single layered. The maximum coupling coefficient is 0.5 when the TET coils are flat against each other without lateral displacement. Such a best coupling condition is used to find the upper frequency boundary of controller. The nominal load of the heart pump is equivalent to 10 Ω. This

translates to a loaded quality factor Q of 5.63 and 1.41 at the primary and secondary circuits respectively. We also investigate a load variation up to 20 Ω to study a severe bifurcated situation. Fig. 5 shows the phase and magnitude sweep of the system with a coupling coefficient of 0.5 and a load equivalent resistance of 20 Ω. Other system parameters are L_p (12 μH), C_p (47 nF), L_s (3 μH) and C_s (168 nF). The equivalent mutual inductance at the highest coupling level is M (3 μH). Applying (1) results in six roots, ±180.26, ±261.37 and ±301.42, however only positive frequencies are practically possible, so the system f_{zvs} are 180.26 kHz, 261.37 kHz and 301.42 kHz. The lowest f_{zvs} is 180.26 kHz, so the upper f_{sw} boundary must be less than 180.26 kHz.

One complication is under bifurcated condition the f_{pk} will be below the lowest f_{zvs}, ideally we should operate below f_{pk}, so a magnitude sweep of circuit V_{LOAD} is conducted giving a f_{pk} of 178.52 kHz, therefore we operate below this f_{pk}.

As a practical verification of the calculated upper frequency boundary for power flow regulation, first let the proposed controller run in open loop, under a desirable dc input voltage (V_{IN}) and the highest expected coupling and loading, we tune f_{sw} upwards toward the theoretical first f_{pk}, by avoiding instant capacitor shorting, the frequency when V_{LOAD} peaks can be set as the upper frequency boundary. The location of theoretical first f_{pk} approximates the practical, the process used to attain the theoretical magnitude curves only considers a situation where the resonant tank is fed with perfect sinusoidal waveforms of different frequencies, while in practice, waveforms will be distorted by differing load, coupling, the resonant tank shorting period and its associated magnitude boosting effect, these factors will deviate the practical magnitude responses from the theoretical and thus changing location of f_{pk}. In addition, practical component drifts and parasitic elements can cause deviations in the practical switching frequency regulation range from the theoretical calculations.

When the coupling is weak and the system is not bifurcated, for example with a coupling coefficient of 0.2 and load of 10 Ω, Fig. 4 shows the phase and magnitude sweep of the system. From (1) the six roots can be obtained as $-224.47 \pm \mathrm{j}419.76$, $224.47 \pm \mathrm{j}419.76$, ±212.75. Clearly only 212.75 kHz is a valid frequency, this frequency is the one and only unique f_{zvs} point for the system to operate under. Note that this f_{zvs} is 30 kHz higher than the upper boundary operating frequency corresponding to the closest coupling and bifurcated situation. From Fig. 5, it can be seen that the first peak magnitude corresponding to f_{pk1} is about 5 dB lower than the non-bifurcated situation. However, this is not an issue in the system design as long as the system can deliver the rated output power even when the system is bifurcated.

When accounting for component variations and other factors, a frequency margin is needed in practical design to ensure the system can work properly. This may affect the system full power capability and the power efficiency slightly.

The lower f_{sw} boundary can be found empirically by operating the controller in open loop. The f_{sw} should be decreased away from the fully tuned state. The f_{sw} boundary will be when output voltage reaches a minimum and begin to rise. However in practice the lower boundary need not be at its theoretical minimum and can be set sufficiently low to allow enough room to regulate power flow downwards. In addition, as frequency lowers the magnitude boosting effect causes higher voltage rating requirement for primary MOSFETs.

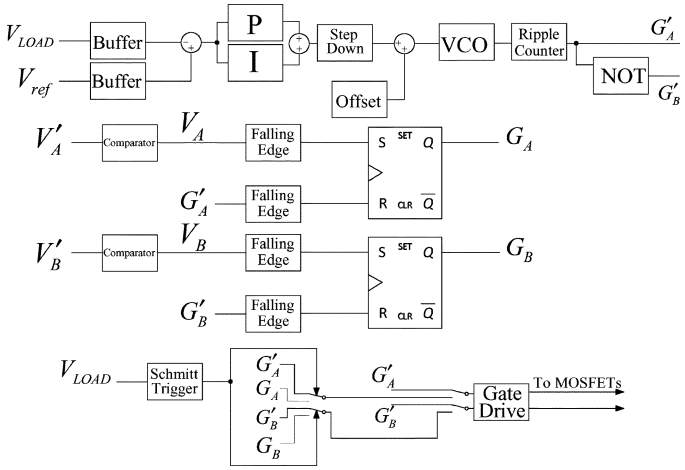

Fig. 7. Controller details.

B. PI Controller Parameters

The PI controller achieves regulation when V_{LOAD} equals V_{ref} through online tracking, important parameters that influence this process include the f_{sw} regulation range, V_{IN}, coupling level and the output load. V_{IN} should be chosen such that the frequency controller has a margin to vary the power flow up or down in order to achieve regulation. We first determine the f_{sw} regulation range according to previous analysis, then while the system operates under close loop, we push the TET coils flat against each other for the highest coupling level, then increase V_{IN} so that PI action starts to regulate V_{LOAD} to V_{ref} by decreasing the frequency downwards, stop increasing V_{IN} when f_{sw} equates to the desired lower boundary of the f_{sw} regulation range. This procedure ensures that the system is capable of regulating voltage down to V_{ref} under highest coupling level, and as the coupling level drops by separating the TET coils, PI action will increase f_{sw} to deliver more power, until the separation distance becomes too great to maintain V_{ref} at the load.

C. Controller Hardware Design

The new controller as shown in Fig. 7 has a PI to vary frequency and regulate the output power flow. This controller was built with discrete analogue components using OPAMPs, VCO and NAND gates. The OPAMPs achieves the needed buffering, differencing, summing, offsetting, proportional gain and integral gain functions of the PI controller, the PI output is stepped down through a potentiometer and an offset voltage is added to complete the necessary frequency range level shifting, the resulting dc voltage level is processed by a VCO into a square wave, which is not 50% duty cycle, so a ripple counter can be used to half the frequency of the VCO output in order to produce a 50% duty cycle waveform. NAND gates are used to realise the required NOT gate function in order to produce the complement of the VCO output resulting in G'_A and G'_B, which are two complementary 50% duty cycle basic mode gate driving signals.

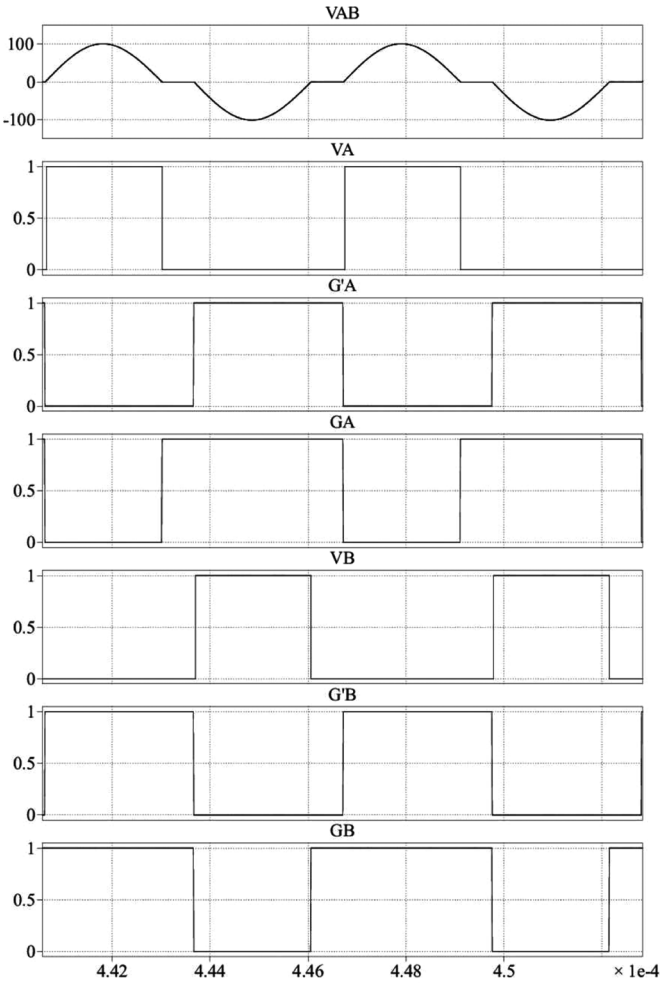

Fig. 8. Simulation waveforms.

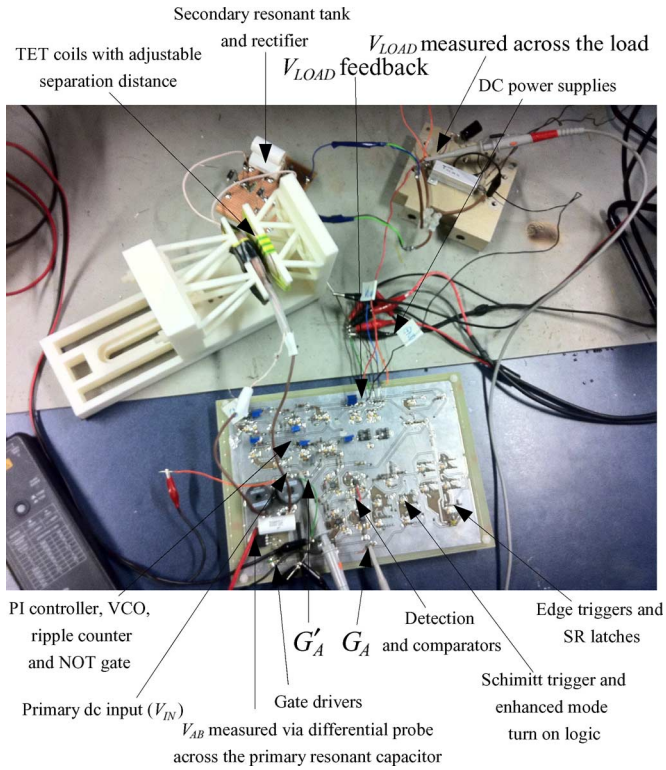

Fig. 9. Practical measurement setup.

To generate MOSFET overlap conducting enhanced mode gate drive signals, G_A and G_B, the falling edge of V_A is used to set a SR latch while a falling edge of G'_A resets that SR latch producing G_A, similarly a falling edge of V_B sets a second SR latch while a falling edge of G'_B resets the second SR latch producing G_B. The enhanced mode waveforms will step in after V_{LOAD} is above a threshold as it relies on the readiness of the basic mode waveforms, G'_A and G'_B, as well as the comparator waveforms V_A and V_B. This design has used only discrete components to realise all the necessary elements of the power flow controller, however microcontrollers or FPGA can also be used to realise the controller.

V. Simulation and Experimental Results

PLECS has been used to simulate the proposed controller and its PI action used to regulate the output voltage to 10 V, the system switching frequency regulation range has been calculated according to the previous analysis and set to 140 kHz to 178.52 kHz, the simulated V_{IN} range for which regulation is achievable is between 23 V and 28 V for a load of 10 Ω and a 0.2 coupling coefficient.

Similarly, simulation was undertaken using PLECS under different coupling and load variations, in all cases the calculated f_{sw} regulation range was used and V_{IN} set at 25 V, the coupling regulation range is between 0.19 to 0.23 for a load of 10 Ω, while the simulated load regulation range is between 7 Ω and 50 Ω for a 0.2 coupling coefficient. If the f_{sw} regulation range were to increase by lowering the f_{sw} lower boundary, the simulated V_{IN}, coupling and load regulation ranges would also increase, that is increases in the f_{sw} regulation range leads to increased controller regulation capability. The simulated regulation ranges are guides for the practical system, they do not represent actual practical ranges.

Practical TET systems require a regulated power of typically 10 W at the heart pump, the power flow controller must overcome variations in TET coil separation and misalignment due to patient movement, which corresponds to variations in coupling level between primary and secondary. A 10 Ω load is used to approximately model a working heart pump. The practical switching frequency regulation range is between 149.3 kHz to 182.2 kHz. The proposed controller has demonstrated good power regulation of 10 W to the load with a TET coil separation ranging from 4 mm to 10 mm. Note that the minimum distance of 4 mm actually corresponds to the best coupling situation with the two coils touching, and the distance is caused by the silicone encasing. The 10 mm distance is the lowest coupling level for maintaining the rated power delivery. Normally the system operates in a non-bifurcated condition, however when the TET coils are less than about 5 mm from each other, system may bifurcate. Under both non-bifurcated and bifurcated conditions the practical system continues to work well below the first f_{pk} within its f_{sw} regulation range and avoids instant capacitor shorting.

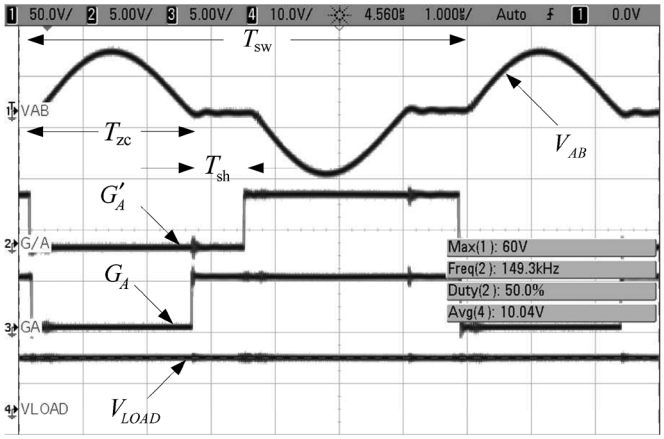

Fig. 10. Practical circuit waveforms, TET coil separation of 4 mm.

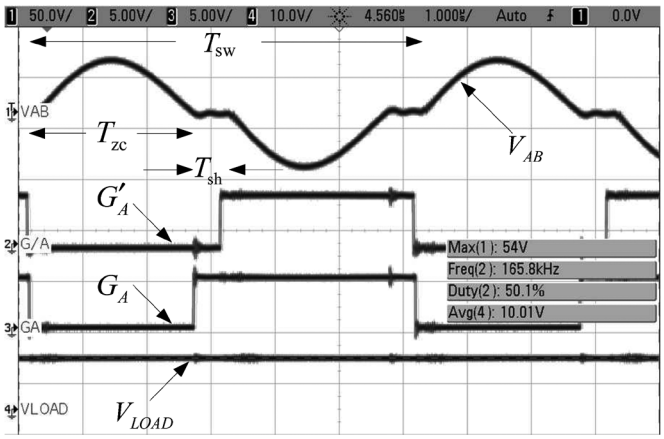

Fig. 11. Practical circuit waveforms, TET coil separation of 7 mm.

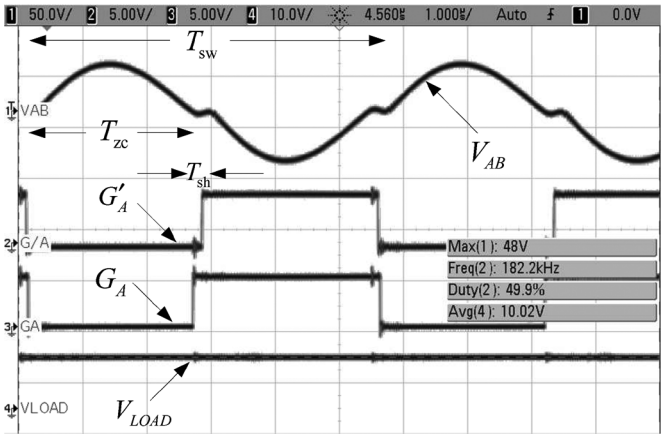

Fig. 12. Practical circuit waveforms, TET coil separation of 10 mm.

The PLECS simulation circuit waveforms are shown in Fig. 8, the practical measurement setup is shown in Fig. 9, and the practical circuit waveforms of three different TET coil separation distances are shown in Fig. 10, Fig. 11 and Fig. 12 under an input dc voltage of 14 V. Note that in all cases the system was able to maintain 10 V at the load side. It is clear that the practical measurement waveforms correspond well to the simulation circuit waveforms and to the ideal circuit waveforms illustrated in Fig. 2. In all three practical circuit waveform figures, the top waveform is the differential resonant tank voltage, V_{AB}, the second waveform is the VCO output or basic gate driving mode waveform, G'_A, the next waveform is the enhanced mode gate driving waveforms, G_A and the last waveform is the load voltage, V_{LOAD}. The circuit currently operates in enhanced mode, operation under basic gate driving mode will give similar results, but due to body diode conduction during resonant tank shorting period the efficiency drops slightly.

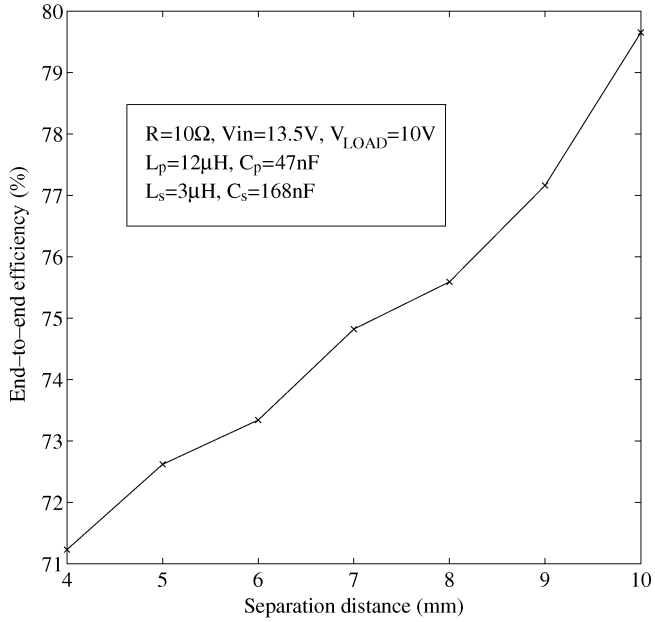

Fig. 13. End-to-end efficiency versus separation distance (enhanced mode).

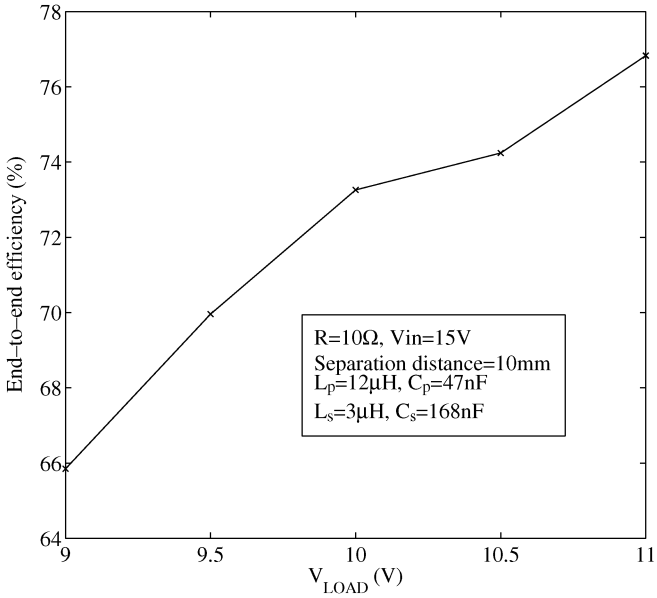

Fig. 14. End-to-end efficiency versus V_{LOAD} (enhanced mode).

The basic gate driving mode has achieved an end-to-end efficiency of 77.97% compared to 79.65% with the enhanced gate driving mode when delivering 10 W at TET coil separation of 10 mm. Fig. 13 shows the end-to-end efficiencies for enhanced mode operation under different direct separation distances, where the system is operating with close loop feed-

back to regulate V_{LOAD} at 10 V. Fig. 14 shows the end-to-end efficiencies for enhanced mode under different V_{LOAD} by operating the system in open loop and varying the operating frequency. These efficiencies do not include controller power losses as the controller components are fed by separate ± 15 V and ± 5 V supplies. The end-to-end efficiency with controller loss is estimated to be above 70%.

VI. Conclusions

A new power flow control method based on resonant tank shorting has been proposed and developed for heart pump applications. The system has been analysed to determine the switching frequency regulation range to avoid instant capacitor shorting during operation. The system has reduced the total component counts compared to the existing frequency controllers. The realised power flow controller has demonstrated good power flow regulation under both non-bifurcated and bifurcated operating conditions.

References

[1] W. L. Holman, J. K. Kirklin, D. C. Naftel, R. L. Kormos, P. Desvign-Nickens, M. T. Camacho, and D. D. Ascheim, "Infection after implantation of pulsatile mechanical circulatory support devices," *J. Thorac. Cardiovasc. Surg.* vol. 139, no. 6, pp. 1632–1636, 2010 [Online]. Available: http://jtcs.ctsnetjournals.org/cgi/content/abstract/139/6/1632

[2] D. M. Budgett, A. P. Hu, P. Si, W. T. Pallas, M. G. Donnelly, J. W. T. Broad, C. J. Barrett, S.-J. Guild, and S. C. Malpas, "Novel technology for the provision of power to implantable physiological devices," *J. Appl. Phys.* vol. 102, no. 4, pp. 1658–1663, 2007 [Online]. Available: http://jap.physiology.org/content/102/4/1658.abstract

[3] A. Karalis, J. Joannopoulos, and M. Soljacic, "Efficient wireless non-radiative mid-range energy transfer," *Ann. Phys.* vol. 323, no. 1, pp. 34–48, 2008 [Online]. Available: http://www.sciencedirect.com/science/article/pii/S0003491607000619

[4] A. Kurs, A. Karalis, R. Moffatt, J. D. Joannopoulos, P. Fisher, and M. Soljacic, "Wireless power transfer via strongly coupled magnetic resonances," *Science* vol. 317, no. 5834, pp. 83–86, 2007 [Online]. Available: http://www.sciencemag.org/content/317/5834/83.abstract

[5] T. Dissanayake, D. Budgett, P. Hu, and S. Malpas, "Experimental thermal study of a tet system for implantable biomedical devices," in *Proc. IEEE Biomedical Circuits and Systems Conf.*, Nov. 2008, pp. 113–116.

[6] T. Dissanayake, A. Hu, S. Malpas, L. Bennet, A. Taberner, L. Booth, and D. Budgett, "Experimental study of a tet system for implantable biomedical devices," *IEEE Trans. Biomed. Circuits Syst.*, vol. 3, no. 6, pp. 370–378, 2009.

[7] P. Si, A. Hu, S. Malpas, and D. Budgett, "A frequency control method for regulating wireless power to implantable devices," *IEEE Trans. Biomed. Circuits Syst.*, vol. 2, no. 1, pp. 22–29, 2008.

[8] D. Thrimawithana, U. Madawala, and P. Lunenburg, "A novel buck-boost control technique for push-pull parallel-resonant converters," in *Proc. IEEE 32nd Annu. Conf. Industrial Electronics*, 2006, pp. 2805–2811.

[9] D. Thrimawithana and U. Madawala, "Analysis of split-capacitor push-pull parallel-resonant converter in boost mode," *IEEE Trans. Power Electron.*, vol. 23, no. 1, pp. 359–368, 2008.

[10] D. Thrimawithana and U. Madawala, "Analysis of split-capacitor push-pull parallel resonant converter in normal mode," in *Proc. Int. Symp. Power Electronics, Electrical Drives, Automation and Motion*, 2008, pp. 778–783.

[11] U. Madawala and D. Thrimawithana, "Mathematical model for split-capacitor push-pull parallel resonant converter in buck mode," *IET Power Electron.*, vol. 1, no. 3, pp. 356–367, 2008.

[12] U. Madawala and D. Thrimawithana, "Operation of a split-capacitor push-pull parallel resonant converter in buck mode," in *Proc. IEEE 33rd Annu. Conf. Industrial Electronics Society*, 2007, pp. 1586–1591.

[13] A. Hu, "Selected resonant converter for IPT power supplies," Ph.D. dissertation, The University of Auckland, Aukland, New Zealand, 2001.

[14] C. Liu and A. Hu, "Steady state analysis of a capacitively coupled contactless power transfer system," in *Proc. IEEE Energy Conversion Congress and Expo.*, Sep. 2009, pp. 3233–3238.

[15] C. S. Tang, Y. Sun, Y. G. Su, S. K. Nguang, and A. Hu, "Determining multiple steady-state zcs operating points of a switch-mode contactless power transfer system," *IEEE Trans. Power Electron.*, vol. 24, no. 2, pp. 416–425, Feb. 2009.

[16] Y. Wu, A. Hu, D. Budgett, S. Malpas, and T. Dissanayake, "Efficient power-transfer capability analysis of the tet system using the equivalent small parameter method," *IEEE Trans. Biomed. Circuits Syst.*, vol. 5, no. 3, pp. 272–282, Jun. 2011.

[17] C.-S. Wang, G. Covic, and O. Stielau, "Power transfer capability and bifurcation phenomena of loosely coupled inductive power transfer systems," *IEEE Trans. Ind. Electron.*, vol. 51, no. 1, pp. 148–157, Feb. 2004.

Bob Wang (S'09) received the B.Sc.(Hons.) degree in electrical and electronic engineering in 2009 from The University of Auckland, Auckland, New Zealand, in 2009.

Currently, he is working toward the Ph.D. degree at The University of Auckland, researching "Efficient Wireless Power Supply for Heart Assist Devices."

Aiguo Patrick Hu (M'98–SM'07) received the B.E. and M.E. degrees from Xian JiaoTong University, Xian, China, in 1985 and 1988 respectively, and the Ph.D. degree from The University of Auckland, Auckland, New Zealand, in 2001.

He was a Lecturer and Director of the China Italy Cooperative Technical Training Center, Xian, China, and later was the General Manager of a technical development company. He holds six patents in inductive power transfer and microcomputer control technologies, has authored many referred journal and conference papers, authored a monograph on wireless/contactless power transfer, and has contributed to book chapters on electrical machines and inductive power transfer control. Currently, he is a Senior Lecturer with the Department of Electrical and Electronic Engineering, The University of Auckland. His research interests include wireless/contactless power transfer, power converters, and the application of power electronics in renewable power systems.

Dr. Hu is the Chairman of IEEE New Zealand North PES (Power and Engineering) and PELS (Power Electronics) Joint Chapter.

David Budgett received the Ph.D. degree in biomedical engineering from Imperial College London, London, U.K., in 1995.

He has held academic positions at the University of Sussex, Sussex, U.K., and The University of Auckland, Auckland, New Zealand, with research interests in medical devices. He leads a team developing implantable telemetry devices at the Bioengineering Institute, The University of Auckland. He is a Founder of the company TETCor, Auckland, New Zealand, which provides wireless power solutions for medical devices.